J Electroceram (2010) 25:11–19
DOI 10.1007/s10832-009-9583-x

Modeling of sensing and transduction for p-type semiconducting metal oxide based gas sensors

N. Barsan · C. Simion · T. Heine · S. Pokhrel · U. Weimar

Received: 6 February 2009 / Accepted: 3 June 2009 / Published online: 16 June 2009

Abstract The development of a quantitative model that correlates conduction in and sensing with *p*-type gas sensitive metal oxides is presented here. The theoretical results are confronted with the experimental data and found to be in very good agreement. The model also explains the differences between the performance of gas sensors based on *n* and *p*-type metal oxides and indicates the possible improvement routes.

Keywords Chemical sensors · Conduction models · p-type · Metal oxide · Gas sensors

1 Introduction

Conductometric gas sensors based on semiconducting metal oxides are actually one of the most investigated groups of gas sensors because of their: low cost and flexibility associated to their production; the simplicity of their use; the large number of detectable gases/possible application fields [1–4]. After it was discovered that there is an electrical effect of the metal oxide-gas reaction—Heiland [5], Bielanski et al. [6] and Seiyama et al. [7]—Taguchi made the decisive step of bringing to the market semiconducting metal oxide based sensors for flammable/explosive gases detectors (SnO_2 based Taguchi-type sensors [8]). It was a success and, nowadays, there are many companies offering this type of sensors, such as Figaro, FIS, MICS, UST, CityTech, AppliedSensors, NewCosmos, etc [9]. Their current applications span from "simple" explosive or toxic gases alarms (see information provided by the gas sensors manufacturers on their homepages) to air intake control in cars [10] to components in complex chemical sensor systems [11]. Most of the companies still use SnO_2 based sensing materials; also employed in commercial applications are WO_3, Ga_2O_3, which are *n-type* semiconductors, and $Cr_{2-x}Ti_yO_{3+z}$, which is a *p-type* semiconductor. In R&D the situation is somehow similar; any survey of the contributions in the field of metal oxide based sensors presented at the most recent major sensors conferences (Eurosensors and International Meeting on Chemical Sensors) will show that, by far, even after more than 30 years of commercial use, SnO_2 is still the most investigated gas sensing material and CO, NO_2 and volatile organic compounds (VOC) the main target gases. The second most studied material is WO_3 while the other industrially used materials are practically not investigated anymore. Accordingly, most of the experimental and theoretical knowledge was gained on SnO_2 [1, 2] and all modelling of, e.g. sensing and transduction, is focused on the *n-type* case [12]. Recently, [13], we investigated the way in which surface reactions-induced electrical changes are affecting the sensor signals of thick porous layers of Cr_2O_3, a *p-type material*, by using simultaneous DC and work function changes (Kelvin probe method) as well as AC impedance spectroscopy measurements; on their basis we developed a conduction model, which qualitatively explains the experimental data. The most important finding, the validity of which should apply to all *p-type* metal oxides used as gas sensitive materials, is that the use of the sensing layer resistance changes as sensor output downgrades the sensor performance for that type of materials. The reason is the way in which the conduction takes place that adds to the measured gas sensitive resistance of the oxide's surface depleted layer the gas insensitive resistances of its bulk, in

N. Barsan (✉) · C. Simion · T. Heine · S. Pokhrel · U. Weimar
University Of Tuebingen,
Tübingen, Germany
e-mail: nb@ipc.uni-tuebingen.de

parallel, and of the contact resistance between the semiconductor and the electrode, in series. In [13] we were not able to quantitatively analyze the experimental data because the modeling of conduction in gas sensitive *p*-type oxides was not available. Here, we are proposing such a model and we are using it in order to extract the relevant material parameters.

2 Sensing and transduction

For semiconducting metal oxide based gas sensors the cause of the change of sensor resistance (sensor signal) is the transfer of free charge carriers (electrons or holes) from/to the semiconductor to/from an adsorbed surface species. Due to the fact that most gas sensing applications are taking place in the ambient atmosphere, a very important role is played by oxygen and water vapors. In a certain temperature range, which depends on the specific metal oxide, the adsorption of oxygen involves the trapping of electrons from the semiconductor; the result will be a decrease of the free charge carriers' concentration (electrons) in the case of n-type semiconductors—e.g. SnO_2, In_2O_3, WO_3—or an increase of the free charge carriers' concentration (holes) in the case of p-type semiconductors—e.g. Cr_2O_3, NiO, CoO. There are cases in which the reaction with ambient oxygen even changes the type of conduction at the surface of the metal oxide [14].

It is generally thought that the reaction of reducing gases with pre-adsorbed oxygen is responsible for the change in resistance of the sensors and also that the presence of pre-adsorbed water vapors-related species influences the reaction. There is evidence that this is not the only way in which reducing gases interact with the metal oxides [15], but a more detailed discussion on the way in which the surface reactions take place goes beyond the scope of this contribution. Here, we want to devise a conduction model that links the changes of the surface charge to the measured resistance of the sensor. For doing so, we will consider that, as already discussed in [13], the main effect of the exposure to reducing gases is the decrease of the negative charge trapped at the surface of the semiconductor in the form of oxygen ions. Figure 1 *middle*, depicts what happens at the surface of a p-type semiconducting metal oxide when electrons from the valence band are captured on the surface traps considered to be associated to the adsorption of ambient oxygen as oxygen ions: one records an increase of the concentration of holes in the vicinity of the surface—build-up of an accumulation layer—described in the energy bands representation as an upward band bending; as a consequence, the electrical resistance of that layer decreases in comparison with the flat bands situation (case depicted in

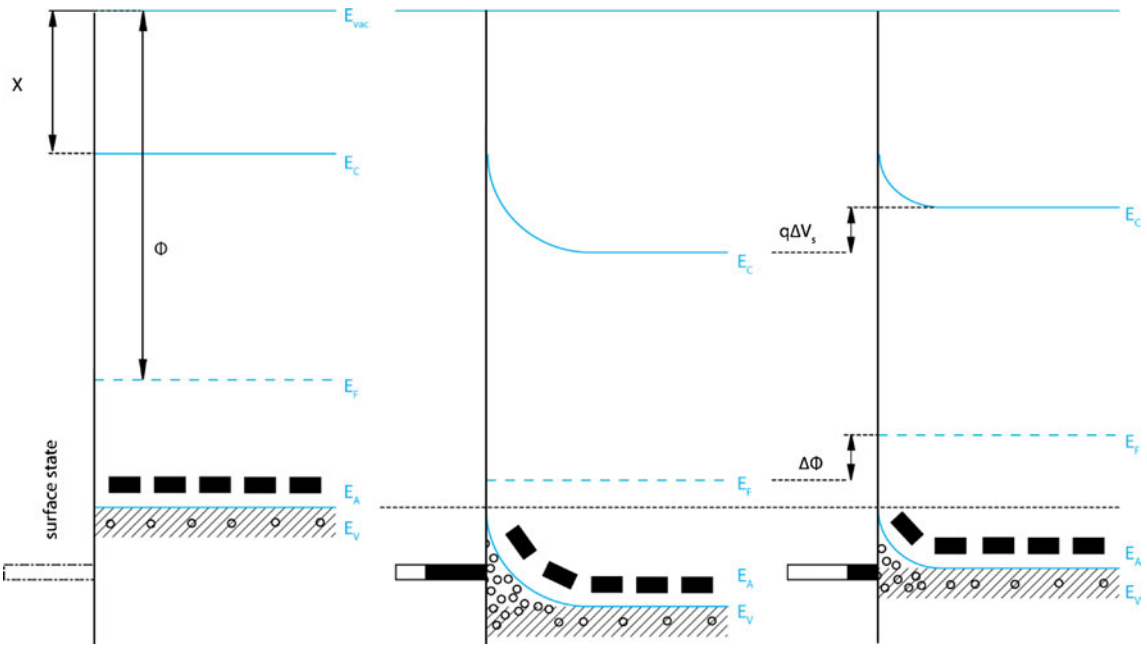

Fig. 1 Energy bands representation of the surface processes associated to the reaction with ambient oxygen and reducing gases: *left*, the flat band situation prior to any surface reaction; *center*, the trapping of electrons due to oxygen adsorption and the formation of the holes accumulation layer; right, the decrease of the surface charge associated to the decrease of adsorbed oxygen ions following the reaction with the reducing gas. E_{VAC} is the energy level of the electrons far away from the semiconductor; E_C is the minimum of the conduction band; E_V is the maximum of the valence band; E_A is the energy level of the intrinsic acceptors; Φ is the work function and χ is the electronic affinity of the semiconductor

Fig. 1 *left*). Figure 1 *right* describes the situation after the exposure to reducing gases has decreased the concentration of oxygen ions: the decrease of the surface negative charge, described in the energy bands representation as an downward band bending ($q\Delta V_S = \Delta\Phi$ in the Figure), determines a decrease of the hole concentration resulting in the increase of the resistance of the accumulation layer. As already demonstrated in [13], the sensor resistance will be the result of the combination between the contributions of the resistances of the surface accumulation layer, bulk and contacts between the electrodes and the semiconductor. The particular manner in which those different contributions are combined depends on the morphology of the sensitive layer; moreover, in the case of the experimental results presented in [13] it was possible to identify the contribution of the electrode-semiconductor contact as a parallel (RC) element in the equivalent circuit that fits the AC impedance spectra; its identification was made possible by the fact that the values of the resistance and capacitance do not change upon exposure to gases. This fact makes it possible to extract out of the data the contribution of the sensing layer and confront it with a conduction model.

To devise a conduction model we need to make some assumptions that will simplify the calculations but also capture all relevant contributions. We will examine a system consisting of loosely aggregated grains in contact with each other but not sintered together (absence of open necks, as defined in [12]). A cartoon description of the sensing layer is presented in Fig. 2. There, the morphological features of the sensing layer are presented together with their corresponding energy bands representations and the corresponding contributions to the overall layer resistance. The generic contributions of the metal-semiconductor contacts are labeled with A and C, and the contribution of the semiconductor grain-grain contacts is labeled with B. The upper part of the figure provides more details on the valence band accumulation layers, on the one hand, determined by the upper band bending at the metal-semiconductor contact due to the difference in work function between the two materials, and, on the other hand,

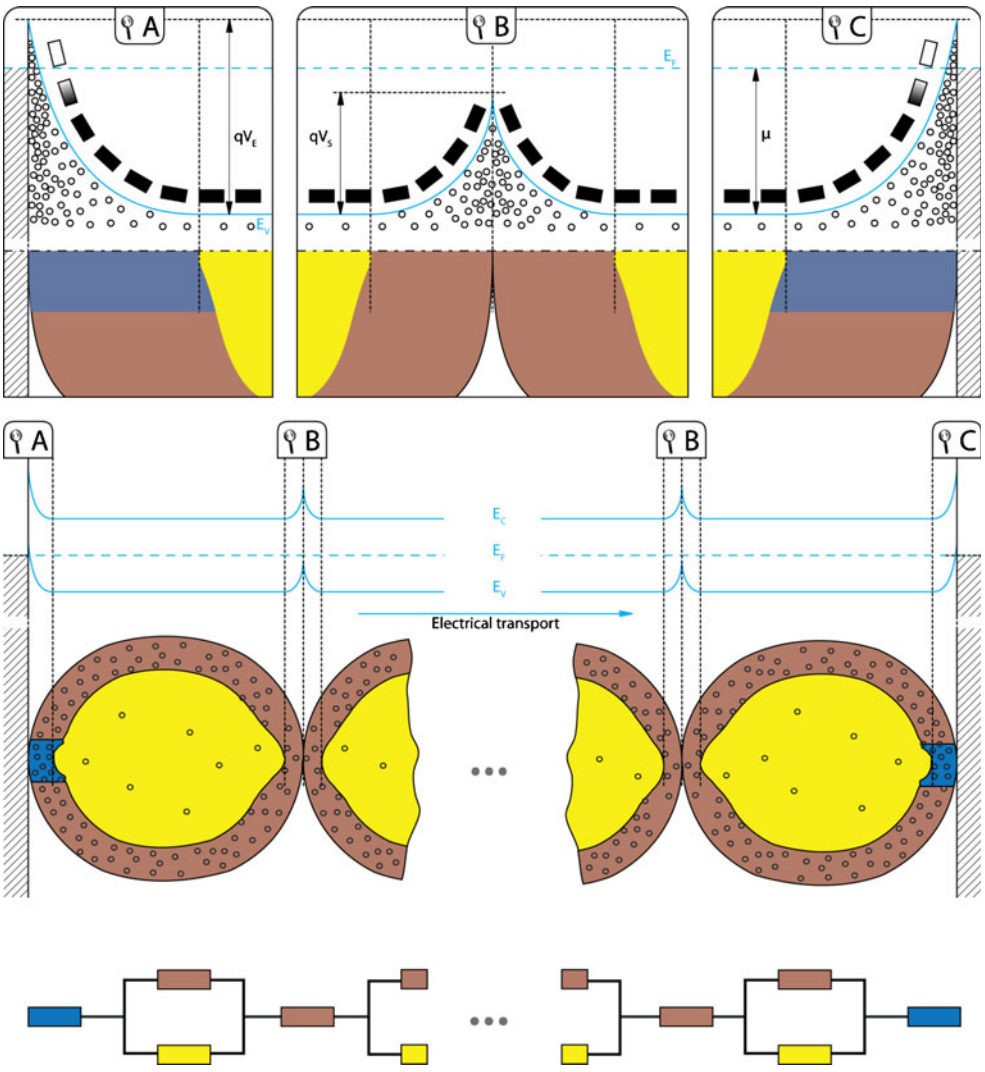

Fig. 2 Cartoon representation of the sensing layer: *center*, simplified depiction of the relevant sensing layer elements, namely the metal-semiconductor contacts (**a** and **c**) and the grain-grain contacts (**b**). The energy bands are constructed on the basis of Fig. 1; *upper part*, zoom-in into the relevant contact regions; *lower part*, equivalent DC circuit

the upper band bending determined by the oxygen adsorption at the ambient exposed grain surfaces. For simplicity sake it was considered that the work function of the metal is higher; from the point of view of the contribution to the overall sensing layer resistance, due to the fact that the metal-semiconductor resistance does not change under gas exposure [12, 13], it does not make any difference if the opposite situation is encountered. In the lower part of Fig. 2, the corresponding equivalent DC circuit is sketched; it is important to recognize that we have four types of contributions:

- The ones of the metal-semiconductor contact, which are in series with all the others;
- The ones of the outer conductive and narrow accumulation layers at the surface of the grains and of the resistive but broad bulk of the grains. They are in parallel to each other and in series with the metal-semiconductors contribution and the
- Grain-grain contacts, which are putting together two accumulation layer regions.

Such a system gives a good description for most state of the art semiconducting MOX gas sensors that are based on porous, thick films realized from pre-processed powders.

For a first step, we will consider that the building blocks of the model are cubic metal oxide grains (grain size D, see Fig. 3(a)) and we will not discuss the contribution of the metal-semiconductor contacts. The grains consist of a relatively (when compared to the grain size) thin conductive skin (thickness x_0) and a more resistive bulk. In the case of a grain fully contacted on two opposed faces, an electrical current passing from one side to the opposite one will experience three types of resistors (see Fig. 3(b)): $R_{1,\,4}$, corresponding to the conductive regions of the cube's faces through which the current enters and leaves the grain, R_2, corresponding to the outer conductive layer and R_3, corresponding to the bulk. In fact, $R_{1,\,4}$ represent the contribution to the grain resistance of its contacts to the other grains in the sensing layer and also the only regions affected by the surface processes that the current is obliged to pass through. After leaving those regions the current can divide between the bulk and the surface and the specific way in which this will happen and, as a consequence, the degree to which the surface processes influence the overall resistance, depends on both geometrical characteristics of the grain (D), reactivity of the surface and bulk properties (grouped together in x_0). The grain resistance, R, is (Fig. 3(c)):

$$R = R_1 + \frac{R_2 \cdot R_3}{R_2 + R_3} + R_4 \tag{1}$$

One can easily calculate all contributions to grain resistance, R, in the hypothesis that ($D >> x_0$):

$$R_1 = \frac{1}{q \cdot \mu \cdot \widetilde{p}_S} \cdot \frac{x_0}{D^2} = R_4 \tag{2}$$

$$R_2 = \frac{1}{q \cdot \mu \cdot \widetilde{p}_S} \cdot \frac{D - 2 \cdot x_0}{D^2 - (D - 2 \cdot x_0)^2} \approx \frac{1}{q \cdot \mu \cdot \widetilde{p}_S} \cdot \frac{1}{4 \cdot x_0} \tag{3}$$

$$R_3 = \frac{1}{q \cdot \mu \cdot p_B} \cdot \frac{D - 2 \cdot x_0}{(D - 2 \cdot x_0)^2} \approx \frac{1}{q \cdot \mu \cdot p_B} \cdot \frac{1}{D} = R_B \tag{4}$$

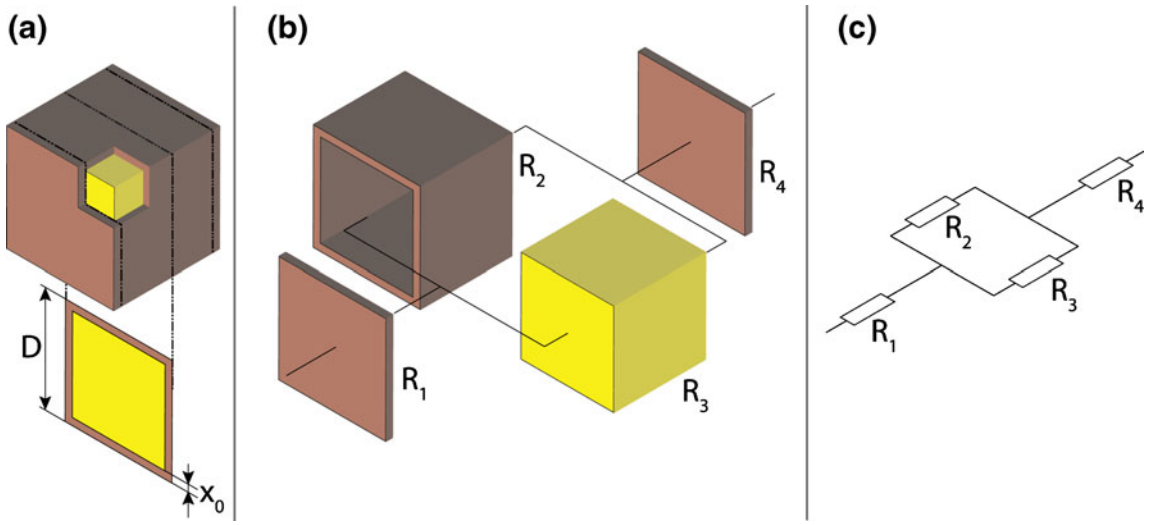

Fig. 3 Simplified model of the metal oxide grains, used for the calculation of the grain resistance: *left*, the cubic grain model; *center*, sketch of the electrical connection between the different grain parts; *right*, the corresponding DC equivalent circuit of the grain

The formulae above are obtained by considering that the mobility,μ, is the same in all the grain and with $\widetilde{p}_S$ being the average concentration of holes in the accumulation layer.

One can express all resistances as a function of R_B:

$$R_{1,4} = R_B \cdot \frac{p_B}{\widetilde{p}_S} \cdot \frac{x_0}{D} \tag{5}$$

$$R_2 = R_B \cdot \frac{p_B}{\widetilde{p}_S} \cdot \frac{D}{4 \cdot x_0} \tag{6}$$

And the result for the grain resistance is:

$$R = R_B \cdot \left(\frac{2 \cdot x_0}{D} \cdot \frac{p_B}{\widetilde{p}_S} + \frac{1}{1 + \frac{4 \cdot x_0}{D} \cdot \frac{\widetilde{p}_S}{p_B}} \right) \tag{7}$$

In Eq. 7, the first term in parenthesis represents the grain-grain contact, which is a pure "surface", in fact surface layer, contribution and the second term describes the distribution of the current between the bulk and the outer surface region of the grain. The terms that describe the surface effects are $\frac{p_B}{\widetilde{p}_S}$ and x_0. The way in which the surface affects the resistance is determined by the value of the ratio $\frac{x_0}{D}$. Already in Eq. 7 one can observe why the sensitivity of the p-type materials can be very low even if the surface reactivity is very high; high surface effects will mean a high increase of $\widetilde{p}_S$ in comparison to p_B. This will make the first term in Eq. 7 the pure "surface" one, small in comparison with the second one and, in this way, its weight in the grain resistance not significant. In the second term, the importance of the surface will depend strongly on both the geometric balance between x_0 and D and the surface reactivity; for example, if one has a ratio between grain size and accumulation layer depth of a factor 100, which is quite reasonable, we will need an increase of the average surface concentration of holes of a factor 25 to have a halving of the grain resistance.

Equation 7 can be corrected to take into account the fact that the contact between grains is not between two faces, by introducing an effective contact area size, D_C, which can be much smaller than the grain size (see Fig. 4) and of an effective grain size, D_G, which will include the numerical factors (4 in Eq. 7) that are depending on the specific geometry chosen for the modeling (spheres, cylinders, cubes, etc). As a consequence, the geometry of the parallel bulk-surface regions will also be modified from the simple cube-like ones and that will change the numeric factors in the second term of Eq. 7. We think that a good proposal for the grain resistance and, in an effective medium approach, for the sensing layer resistance is:

$$R = R_B \cdot \left(\frac{x_0}{D_C} \cdot \frac{p_B}{\widetilde{p}_S} + \frac{1}{1 + \frac{x_0}{D_G} \cdot \frac{\widetilde{p}_S}{p_B}} \right) \tag{8}$$

It is possible to make explicit the dependence on the surface band bending of the resistance and, by that, decouple the geometric and surface effects. For that we need to calculate $\widetilde{p}_S$. In the case $D >> x_0$, one treats the situation in a planar and semi-infinite manner (one-dimensional problem) and we can write:

$$\widetilde{p}_S = \frac{1}{x_0} \int_0^{x_0} p(x)dx = \frac{1}{x_0} \int_0^{x_0} p_b \exp\left(\frac{qV}{kT}\right) dx \tag{9}$$

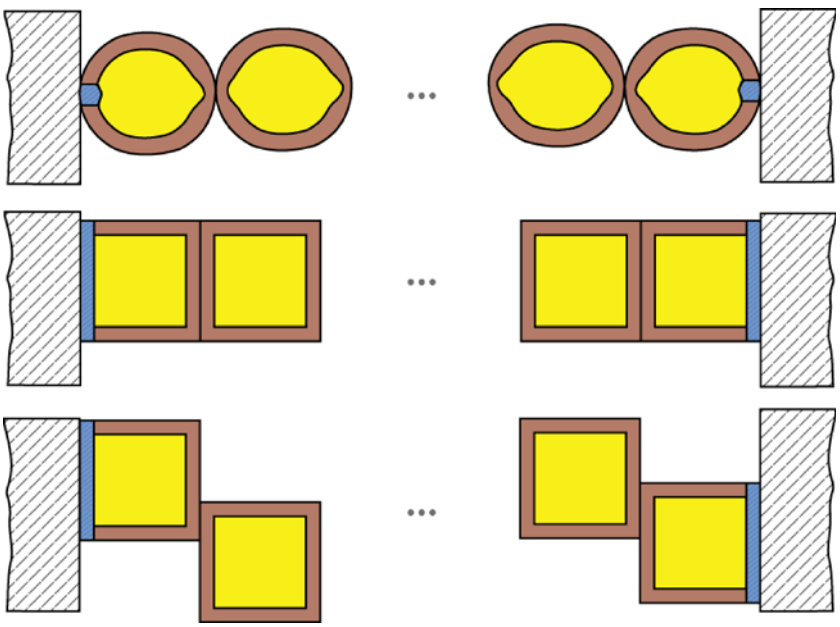

Fig. 4 Sketch of the conduction models used in the theoretical modeling: *upper part*, the actual sensing layer; *center*, the approximation of cubic grains in full contact; *lower part*, the approximation of cubic grains partly in contact

In Eq. 9 the assumption of the Fermi energy still far away from the valence band edge was made in order to be allowed to use the Boltzmann distribution. In order to proceed with the integration we need to:

- change the variable from x to V

$$\widetilde{p}_S = \frac{p_B}{x_0}\int_{V_S}^{0}\frac{\exp\left(\frac{qV}{kT}\right)}{\left(\frac{dV}{dx}\right)}dV \tag{10}$$

- use the results of the first analytical integration of the Poisson's equation for a *p-type* semiconductor [16]

$$\left(\frac{dV}{dx}\right) = \pm\left[\frac{2kT\cdot p_b}{\varepsilon\varepsilon_0}\right]^{1/2}\left[\exp\left(\frac{qV}{kT}\right) - \frac{qV}{kT} - 1\right]^{1/2} \tag{11}$$

to express everything as a function of the potential V. The integral is now:

$$\widetilde{p}_S = \pm\frac{p_b}{x_0}\int_{V_S}^{0}\frac{\exp\left(\frac{qV}{kT}\right)}{\left[\frac{2kT\cdot p_b}{\varepsilon\varepsilon_0}\right]^{1/2}\left[\exp\left(\frac{qV}{kT}\right) - \frac{qV}{kT} - 1\right]^{1/2}}dV \tag{12}$$

By subtracting p_b from both sides of Eq. 12

$$\begin{aligned}\widetilde{p}_S - p_b &= \pm\frac{p_b}{x_0}\int_{V_S}^{0}\frac{\exp\left(\frac{qV}{kT}\right)}{\left[\frac{2kT\cdot p_b}{\varepsilon\varepsilon_0}\right]^{1/2}\left[\exp\left(\frac{qV}{kT}\right)-\frac{qV}{kT}-1\right]^{1/2}}dV - \frac{1}{x_0}\int_{0}^{x_0}p_b dx = \\ &= \pm\frac{p_b}{x_0}\left[\frac{\varepsilon\varepsilon}{2kT\cdot p_b}\right]^{1/2}\int_{V_S}^{0}\frac{\left[\exp\left(\frac{qV}{kT}\right)-1\right]dV}{\left[\exp\left(\frac{qV}{kT}\right)-\frac{qV}{kT}-1\right]^{1/2}}\end{aligned} \tag{13}$$

and by observing that, similarly to the approach used in [17]

$$\begin{aligned}&\frac{d}{dV}\left[\exp\left(\frac{qV}{kT}\right) - \frac{qV}{kT} - 1\right] \\ &\quad = \frac{q}{kT}\cdot\left[\exp\left(\frac{qV}{kT}\right) - 1\right]\end{aligned} \tag{14}$$

one finally obtains for $\widetilde{p}_S$:

$$\begin{aligned}\widetilde{p}_S &= p_b \\ &\cdot\left\{\frac{L_D}{x_0}\sqrt{2}\cdot\left[\exp\left(\frac{qV_S}{kT}\right) - \frac{qV_S}{kT} - 1\right]^{1/2} + 1\right\}\end{aligned} \tag{15}$$

where L_D is the Debye length, a measure of the screening of the bulk from the surface effects [16] and having values close to the ones of x_0, defined as:

$$L_D = \sqrt{\frac{\varepsilon\varepsilon_0 kT}{q^2 p_b}} \tag{16}$$

One can further simplify Eq. (15) by observing that, as shown in Fig. 5 and keeping in mind that $\frac{L_D}{x_0}\sqrt{2} \approx 1$, one can make the approximation

$$\begin{aligned}&\left\{\frac{L_D}{x_0}\sqrt{2}\cdot\left[\exp\left(\frac{qV_S}{kT}\right) - \frac{qV_S}{kT} - 1\right]^{1/2} + 1\right\} \\ &\quad \approx \frac{L_D}{x_0}\sqrt{2}\exp\left(\frac{qVs}{2kT}\right)\end{aligned} \tag{17}$$

for all values of V_S.

By using (8), (15) and (17) one obtains for the sensor layer resistance:

$$\begin{aligned}R &= R_B \\ &\cdot\left(\frac{L_D}{D_C}\cdot\exp\left(-\frac{qV_S}{2kT}\right) + \frac{1}{1+\frac{L_D}{D_G}\cdot\exp\left(\frac{qVs}{2kT}\right)}\right)\end{aligned} \tag{18}$$

Equation 18 is having the advantage that it decouples the surface effects (V_S) from the bulk/material properties (L_D) and morphology (D_C and D_G). It also captures all important parameters that control the dependence of the sensor resistance on the ambient atmosphere composition and clearly shows that the effect of what happens at the surface (changes of band bending V_S) will be felt quite differently for different materials and, for the same materials, different sensing layer morphologies. Some examples are provided in Fig. 6 and 7, where the effect of the geometrical/morphological parameters (L_D/D_C and L_D/D) is examined in the hypothesis of a large variation of band bending. One can see that the most important effect, highest effect of band bending on layer resistance, comes from the grain size reduction.

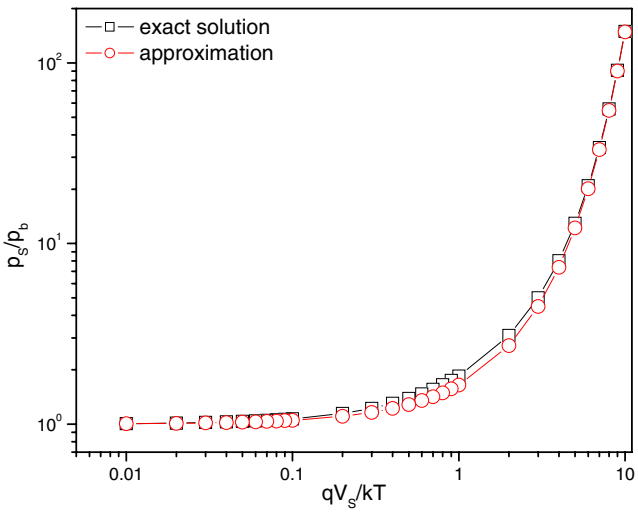

Fig. 5 The dependencies of the normalized surface average hole concentration on band bending for the exact solution (Eq. 15) and the approximate one (Eq. 17)

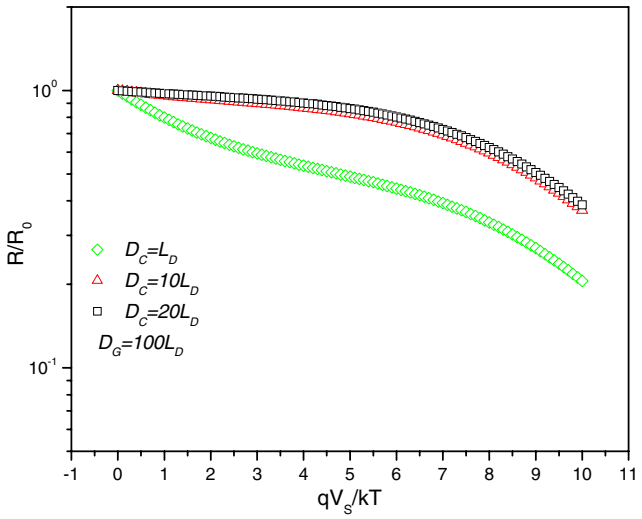

Fig. 6 Influence of the contact size over the sensor response at constant grain size

In the case of *n-type* materials, for a similar layer morphology the term that will dominate the resistance is equivalent of the first term in the brackets of Eq. 18, which provides the large series resistance proportional to $\exp\left(\frac{qV_S}{kT}\right)$[12]. By having the dominant resistive term being the one that depends most strongly on the surface effects, the *n-type* materials will show better gas responses than the *p-type* ones, provided that the surface reactivity and layer morphology are comparable.

3 Discussion

It is interesting to see how good the model proposed by Eq. 18 is by applying it to the results obtained with real sensors. In [13], on the one hand, we performed AC sensor impedance measurements and, on the other hand, we performed simultaneous work function changes and DC sensor resistance measurements. From the former, we have been able to identify and subtract the resistance of the electrode-metal oxide contact; from the latter, we are able to correlate the sensor layer signal—expressed as the ratio between the resistance of the sensor in the presence of ethanol vapors and the resistance of the sensor in air—and the changes in the band bending. According to (18) the sensor signal S is:

$$S=\frac{R_{gas}}{R_{air}}=\frac{\frac{L_D}{D_C}\cdot\exp\left(-\frac{qV_{gas}}{2kT}\right)+\frac{1}{1+\frac{L_D}{D_G}\cdot\exp\left(\frac{qV_{gas}}{2kT}\right)}}{\frac{L_D}{D_C}\cdot\exp\left(-\frac{qV_{air}}{2kT}\right)+\frac{1}{1+\frac{L_D}{D_G}\cdot\exp\left(\frac{qV_{air}}{2kT}\right)}} \tag{19}$$

The measured work function change upon ethanol vapours exposure is:

$$\Delta\Phi=qV_{air}-qV_{gas}\Rightarrow qV_{gas}=qV_{air}-\Delta\Phi \tag{20}$$

so Eq. 19 becomes

$$S=\frac{R_{gas}}{R_{air}}=\frac{\frac{L_D}{D_C}\cdot\exp\left(-\frac{qV_{air}}{2kT}\right)\cdot\exp\left(\frac{\Delta\Phi}{2kT}\right)+\frac{1}{1+\frac{L_D}{D_G}\cdot\exp\left(\frac{qV_{air}}{2kT}\right)\cdot\exp\left(-\frac{\Delta\Phi}{2kT}\right)}}{\frac{L_D}{D_C}\cdot\exp\left(-\frac{qV_{air}}{2kT}\right)+\frac{1}{1+\frac{L_D}{D_G}\cdot\exp\left(\frac{qV_{air}}{2kT}\right)}} \tag{21}$$

With obvious notations, Eq. 21 can be re-written as:

$$S=\frac{R_{gas}}{R_{air}}=\frac{t_1\cdot\exp\left(\frac{\Delta\Phi}{2kT}\right)+\frac{1}{1+t_2\cdot\frac{1}{\exp\left(\frac{\Delta\Phi}{2kT}\right)}}}{t_1+\frac{1}{1+t_2}} \tag{22}$$

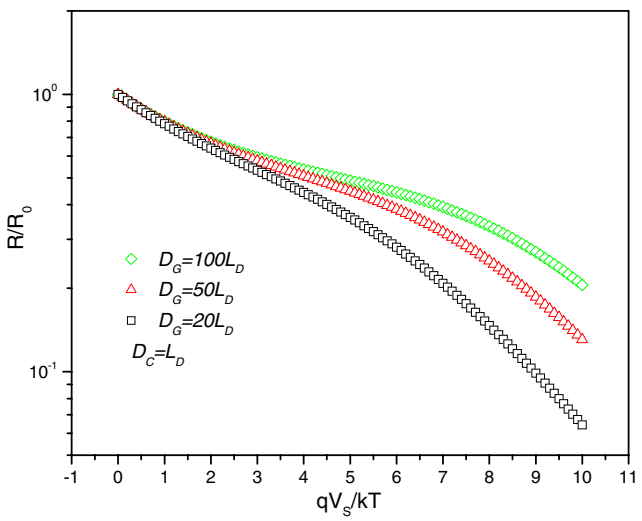

Fig. 7 Influence of the grain size over the sensor response at constant contact size

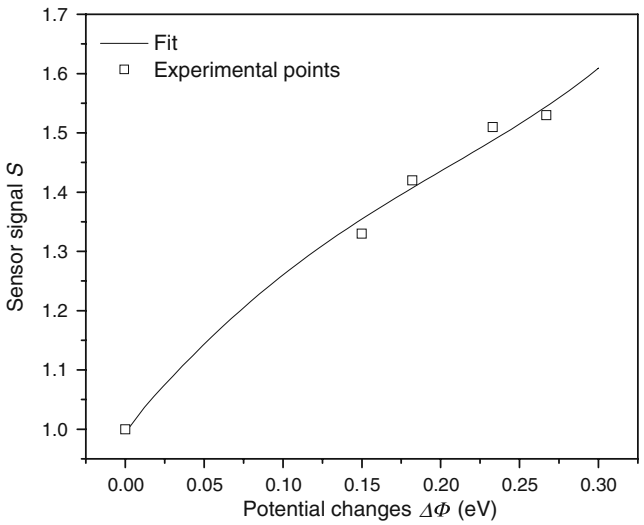

Fig. 8 Dependence of the sensor signal on band bending; experimental results and fitting with the formula described by Eq. 22

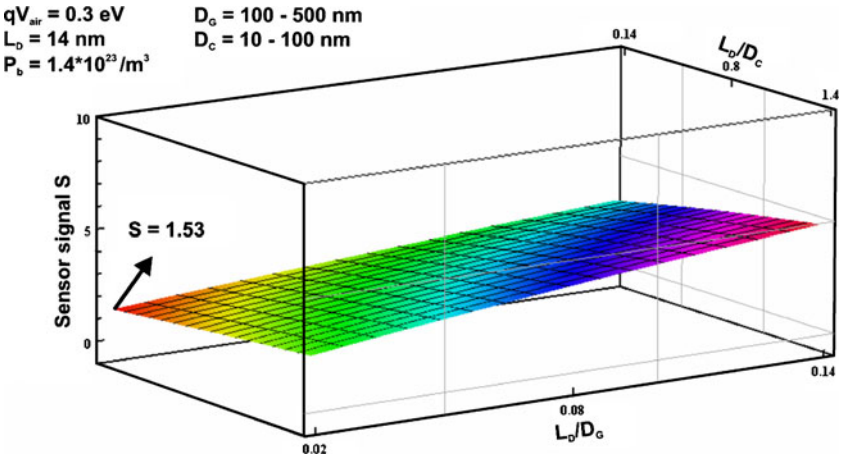

Fig. 9 Simulation of the impact of grain and contact size on the sensor response for a sensitive material that has an initial band bending of 300 meV

The experimental results of the sensor signal dependence on the work function changes are presented in Fig. 8 together with the curve obtained by fitting the data with Eq. 22; the values obtained for the fit parameters are: t_1=0.00762 and t_2=0.47669. To get a feeling about the meaningfulness of the fit parameters we need to make some assumptions; because during ethanol exposure the work function changes were close to 300 meV without recording saturation, we know that the minimal initial bend bending (qV_{air}) should be at least 300 meV. In this case we will obtain for the bulk/morphological parameters (L_D/D_C and L_D/D_G):

$$\frac{L_D}{D_C} = 0.14$$

$$\frac{L_D}{D_G} = 0.02$$

Keeping in mind the fact that the average grain size is around 500 nm, we are obtaining for the Debye length a value of around 14 nm—corresponding to a p_b value of around 1.4×10^{23} m^{-3}, see Eq. 16—and for the size of the grain-grain contact a value of around 100 nm (one fifth of the value of the grain size); the obtained values look reasonable for a semiconducting metal oxide. There are not too many possibilities to compare the values resulting from the fit to directly experimentally determined ones; the values we found in literature for p_b, in a comparable temperature range (280°C) [18] for the case of Cr_2O_3 with induced non-stoichiometry, are around 10^{26} m^{-3}, which would correspond to a value of the initial band bending of about 700 meV; the later value is also reasonable, even if a bit high. Anyways, the values given in [18] seem to be pretty high and in order to match them with the measured conductivity values the author assumes an extremely low value of hole mobility, 3 to 5×10^{-5} cm^2/V s, in full contradiction to the values found by Hauffe and Block [19], namely 0.76 cm^2/V s at a much higher temperature (600°C). On the basis of the information available in the literature it seems reasonable to assume that the initial band bending values are between 300 and 600 meV. For the latter case, the value of the Debye length is around 0.8 nm—corresponding to a p_b value of around 4×10^{25} m^{-3}—and the value of the size of the grain-grain contact a value of around 6 nm (a bit more than one hundredth of the value of the grain size). Figure 9 and 10 present the hypothetical cases in which the grain size (D_G)

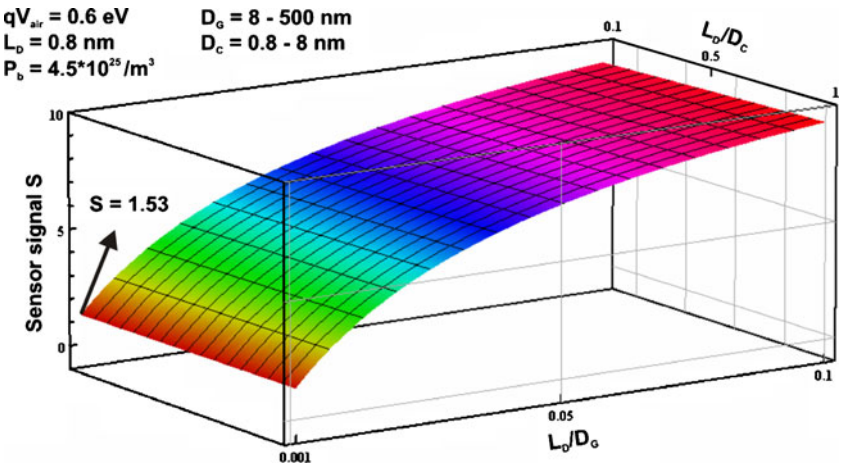

Fig. 10 Simulation of the impact of grain and contact size on the sensor response for a sensitive material that has an initial band bending of 600 meV

and morphology (D_C) of two materials, which are having the bulk properties (L_D) of the two extreme cases considered above, are changed. One can observe that for high effects one needs materials that: are highly reactive to oxygen (high initial band bending); have high concentrations of free charge carriers (low L_D value) and low grain sizes. The effect of morphology, L_D/D_C, is limited in those cases (see Fig. 10). On the opposite, in the case of materials with not so high oxygen reactivity and lower concentration of free charge carriers, the effects of grain size and morphology are comparable (see Fig. 9). In the case of *n*-type materials, the grain size influence over the sensor signal will be limited because the contribution of the non-sensitive part of the grains, the bulk, is limited by its lack of influence in the overall layer resistance (low series resistance) (Fig. 1).

The conduction model developed here has some limitations imposed by the conditions in which it is possible to obtain an analytical solution, mainly $D_G >> L_D$. This fact limits its applicability to "large" grains and excludes the analysis of "fully" enriched materials. The elaboration of a more comprehensive model is currently undertaken.

4 Conclusion

A conduction model valid for *p*-type gas sensitive metal oxides with large grain sizes, when compared to the Debye length, was developed and found to be in good agreement with the experimental results. It provides a quantitative explanation for the low sensor signals of those materials in spite of their high surface reactivity and guidance on how to attempt the improvement of the sensor performance. It also explains the origin of the differences between *n* and *p*-type gas sensitive metal oxides. The boundary conditions in which the conduction model was devised are limiting its applicability and asking for its extension towards materials whose grains are fully influenced by surface reactions.

References

1. D.E. Williams, Semiconducting oxides as gas-sensitive resistors. Sens. Actuators B Chem. **57**, 1–16 (1999). doi:10.1016/S0925-4005(99) 00133-1
2. N. Barsan, M. Schweizer-Berberich, W. Gopel, Fundamental and practical aspects in the design of nanoscaled SnO2 gas sensors. A status report, Fresenius'. J. Anal. Chem. **365**, 287–304 (1999). doi:10.1007/s002160051490
3. G. Korotcenkov, Gas response control through structural and chemical modifications of metal oxide films: state of the art and approaches. Sens. Actuators, B **107**, 209–232 (2005)
4. K. Ihokura and W. J., The stannic oxide gas sensor: principle and application. (CRC, 1994)
5. G. Heiland, Zum Einfluss von Wasserstoff auf die elektrische Leitfähigkeit von ZnO-Kristallen. Z. Phys. **138**, 459–464 (1954). doi:10.1007/BF01340692
6. A. Bielanski, J. Deren, J. Haber, Electric conductivity and catalytic activity of semiconducting oxide catalysts. Nature **179**, 668–669 (1957). doi:10.1038/179668a0
7. T. Seiyama, A. Kato, K. Fujiishi, M. Nagatani, A new detector for gaseous components using semiconductive thin films. Anal. Chem. **34**, 1502f (1962). doi:10.1021/ac60191a001
8. N. Taguchi, in U.S.Patent. 3,631,436, 1971
9. http://www.figarosens.com, http://www.fisinc.co.jp, http://www.appliedsensors.com, http://www.citytech.com, http://www.microchem.com
10. J. Marek, H.-P. Trah, Y. Suzuki, I. Yokomori, *Sensors for automotive technology* (Weinheim, VCH Weinheim, 2003)
11. T.C. Pearce, S.S. Schiffman, H. Troy Nagle, G.J.W., Handbook of machine olfaction: electronic nose technology. (Wiley, 2003)
12. N. Barsan, U. Weimar, Conduction model of metal oxide gas sensors. J. Electroceram. **7**(3), 143–167 (2001). doi:10.1023/A:1014405811371
13. S. Pokhrel, C.E. Simion, V. Quemener, N. Bârsan, U. Weimar, Investigations of conduction mechanism in Cr_2O_3 gas sensing thick films by ac impedance spectroscopy and work function changes measurements. Sens. Actuators, B **133**(1), 78–83 (2008)
14. A. Gurlo, N. Barsan, A. Oprea, M. Sahm, T. Sahm, U. Weimar, A n- to p- type conductivity transition induced by oxygen adsorption on α-Fe2O3. Appl. Phys. Lett. **85**(12), 2280–2281 (2004). doi:10.1063/1.1794853
15. N. Barsan, D. Koziej, U. Weimar, *Metal oxide based gas sensor research: how to? Special Issue, 25th Anniversary of Sensors and Actuators B: Chemical*, E. Bakker, M. Egashira, M. Koudelka-Hep, R. Narayanaswany (Eds.). Sensors and Actuators B 121, 18–35 (2007)
16. S.R. Morrison, *The Chemical Physics of Surfaces* (Plenum, New York, 1977). ISBN 0-306-30960-2, Sec. 2.2
17. N. Bârsan, R. Ionescu, The mechanism of interaction between CO and SnO2 surface—the role of water vapour. Sens. Actuators, B **12**(1), 71–75 (1993)
18. L.N. Cojocaru, Electrical properties of non-stoichiometric Cr_2O_3. Z. physic. Chem. Neue Folg **64**(5/6), 255–262 (1969)
19. K. Hauffe, J. Block, Defective array model of an intrinsic-impurities semiconductor, Cr_2O_3. Z. Phys. Chem. **198**(5/6), 232–247 (1951)